

Novel Genetic Models of Osteoporosis by Overexpression of Human RANKL in Transgenic Mice

Vagelis Rinotas,^{1,2} Alexandra Niti,¹ Romain Dacquin,³ Nicolas Bonnet,⁴ Marina Stolina,⁵ Chun-Ya Han,⁵ Paul Kostenuik,⁵ Pierre Jurdic,³ Serge Ferrari,⁴ and Eleni Douni^{1,2}

¹Laboratory of Genetics, Department of Biotechnology, Agricultural University of Athens, Athens, Greece

²Biomedical Sciences Research Center "Alexander Fleming", Vari, Greece

³Institut de Génomique Fonctionnelle de Lyon, Université de Lyon, CNRS, Ecole Normale Supérieure de Lyon, Lyon, France

⁴Department of Rehabilitation and Geriatrics, Geneva University Hospital and Faculty of Medicine, Geneva, Switzerland

⁵Metabolic Disorders Research, Amgen Inc., Thousand Oaks, CA, USA

ABSTRACT

Receptor activator of NF- κ B ligand (RANKL) plays a key role in osteoclast-induced bone resorption across a range of degenerative bone diseases, and its specific inhibition has been recently approved as a treatment for women with postmenopausal osteoporosis at high or increased risk of fracture in the United States and globally. In the present study, we generated transgenic mice (TghuRANKL) carrying the human RANKL (huRANKL) genomic region and achieved a physiologically relevant pattern of RANKL overexpression in order to establish novel genetic models for assessing skeletal and extraskeletal pathologies associated with excessive RANKL and for testing clinical therapeutic candidates that inhibit human RANKL. TghuRANKL mice of both sexes developed early-onset bone loss, and the levels of huRANKL expression were correlated with bone resorption and disease severity. Low copy Tg5516 mice expressing huRANKL at low levels displayed a mild osteoporotic phenotype as shown by trabecular bone loss and reduced biomechanical properties. Notably, overexpression of huRANKL, in the medium copy Tg5519 line, resulted in severe early-onset osteoporosis characterized by lack of trabecular bone, destruction of the growth plate, increased osteoclastogenesis, bone marrow adiposity, increased bone remodeling, and severe cortical bone porosity accompanied by decreased bone strength. An even more severe skeletal phenotype developed in the high copy Tg5520 founder with extensive soft tissue calcification. Model validation was further established by evidence that denosumab, an antibody that inhibits human but not murine RANKL, fully corrected the hyper-resorptive and osteoporotic phenotypes of Tg5519 mice. Furthermore, overexpression of huRANKL rescued osteoporotic phenotypes of RANKL-defective mice. These novel huRANKL transgenic models of osteoporosis represent an important advance for understanding the pathogenesis and treatment of high-turnover bone diseases and other disease states caused by excessive RANKL. © 2014 American Society for Bone and Mineral Research.

KEY WORDS: BONE; OSTEOPOROSIS; RANKL; ANIMAL MODELS; TREATMENT

Introduction

Bone remodeling is a constant physiological process of bone resorption and formation. Osteoclasts initiate the remodeling cascade by removing bone matrix and subsequently osteoblasts refill these resorption cavities with organic bone matrix, which gradually attains its biomechanical strength and stiffness via mineralization.⁽¹⁾ In the healthy young adult skeleton, osteoblastic and osteoclastic activities are typically balanced so that skeletal integrity is preserved. Osteoporosis is a metabolic disease that is associated with unbalanced bone remodeling resulting from decreased bone formation and/or accelerated bone resorption. As a result, refilling of resorption cavities can be incomplete, leading to progressive bone loss, increased bone fragility, and fracture risk.⁽²⁾

The cause of the increased bone remodeling is multifactorial, but a recently discovered cytokine, receptor activator of NF- κ B ligand (RANKL), constitutes the master regulator of bone resorption.⁽³⁾ RANKL, a type II transmembrane protein from the tumor necrosis factor (TNF) superfamily, binds and activates its cognate receptor RANK as a trimer, and it also exists in a soluble form.⁽⁴⁾ Binding of RANKL to RANK initiates a signaling cascade essential for the differentiation, activity, and survival of osteoclasts^(5,6) and subsequently for osteoclast-induced bone resorption.⁽³⁾ The effects of RANKL are physiologically counterbalanced by the soluble decoy receptor osteoprotegerin (OPG), which inhibits the binding of RANKL to RANK on osteoclast progenitors by sequestering RANKL⁽⁷⁾ and thereby limiting osteoclastogenesis.⁽⁴⁾ RANKL is broadly expressed not only in

Received in original form July 9, 2013; revised form September 10, 2013; accepted September 30, 2013. Accepted manuscript online October 11, 2013.

Address correspondence to: Eleni Douni, PhD, Laboratory of Genetics, Department of Biotechnology, Agricultural University of Athens, Iera Odos 75, Athens 11855, Greece. E-mail: douni@aua.gr

Additional Supporting Information may be found in the online version of this article.

The first two authors as well as the second two authors contributed equally to this work.

Journal of Bone and Mineral Research, Vol. 29, No. 5, May 2014, pp 1158–1169

DOI: 10.1002/jbmr.2112

© 2014 American Society for Bone and Mineral Research

bone cells including osteoblasts, osteocytes, and hyperplastic chondrocytes but also in a wide variety of tissues and specific cells such as spleen, heart, lung, brain, thymus, T and B lymphocytes, or mammary epithelia cells.^(8,9) This expression pattern is consistent with the pleiotropic effects of RANKL in diverse tissues including lymphoid tissue organization, mammary gland development during pregnancy, hormone-driven mammary cancer, cancer metastasis, and thermoregulation.⁽¹⁰⁾

Genetic defects impairing the function of RANKL or RANK both in mice and humans result in severe autosomal recessive osteopetrosis (ARO)⁽¹¹⁾ owing to impaired osteoclast formation, demonstrating that RANKL and RANK are indispensable for osteoclastogenesis. On the other hand, when RANKL overwhelms the effects of OPG, as occurs in OPG-deficient mice⁽¹²⁾ and in postmenopausal osteoporosis,⁽¹³⁾ the imbalance in the bone remodeling process results in bone loss and early-onset osteoporosis. In addition, estrogen or androgen deficiency in humans and rodents leads to increased RANKL expression that is possibly associated with increased bone loss and risk of fractures,^(13,14) providing a rationale for the development of RANKL-targeted therapies. Indeed, clinical trials with denosumab, a fully human IgG2 monoclonal antibody that specifically binds human RANKL (huRANKL) with high affinity, showed an increased bone mass and reduced incidence of fractures in postmenopausal women with osteoporosis⁽¹⁵⁾ and in prostate cancer patients receiving androgen-deprivation therapy.⁽¹⁶⁾ This antibody was recently approved for the treatment of postmenopausal women with osteoporosis and patients developing cancer-related bone loss. However, preclinical studies assessing the efficacy and safety of novel huRANKL inhibitors have been restricted so far to limited animal models expressing either nonhuman primate RANKL⁽¹⁷⁾ or chimeric murine/human RANKL.⁽¹⁸⁾ Importantly, the ability of human RANKL to potently activate murine RANK suggested to us that the creation of human RANKL transgenic mice could provide a useful model for studying high-turnover bone disease and other RANKL-induced pathologies without the need for frequent injections of recombinant human RANKL.⁽¹⁸⁾ In addition, controlled expression of huRANKL in transgenic mice is necessary because constitutive overexpression of soluble RANKL from early development is lethal at the late fetal stage.⁽¹⁹⁾

This initial report provides an extensive characterization of several transgenic mouse lines (TghuRANKL) that overexpress to varying degrees human RANKL in tissues that normally express this cytokine. TghuRANKL mice of both sexes developed early-onset osteoporosis and the severity of the osteoporotic phenotype was directly related to the levels of RANKL expression. Skeletal phenotypes of these mice mimicked moderate to severe human osteoporosis including trabecular bone loss, cortical porosity, and increased bone fragility, which was successfully reversed upon denosumab treatment. These mice represent the first genetic rodent models of osteoporosis involving overexpression of huRANKL, which can be used to facilitate the understanding of RANKL-induced pathologies such as osteoporosis, while also permitting the preclinical evaluation of denosumab and potentially other novel huRANKL inhibitors.

Materials and Methods

Mouse husbandry

Osteopetrotic *Rankl*^{fl^{es}/fl^{es}} mice, which bear a loss-of-function *Rankl* mutation, were previously described.⁽²⁰⁾ These and other mice were maintained and bred under specific pathogen-free

conditions in the animal facility of BSRC "Alexander Fleming". All animal procedures were approved and carried out in strict accordance with the guidelines of the Institutional Animal Care and Use Committee and the Region of Attica Veterinarian Office.

Generation and genotyping of RANKL transgenic mice

For the generation of huRANKL transgenic mice, a Not I fragment of 200 kb containing the huRANKL gene was isolated from a human genomic BAC clone (RP11-86N24, ImaGenes GmbH, Berlin, Germany) with pulse field gel electrophoresis. The excised band was subsequently run in 4% low melting agarose gel and isolated with β -agarase (New England Biolabs, Hitchin, UK) digestion. After dialysis in microinjection buffer, the transgene was microinjected into the pronuclei of fertilized (C57BL/6J \times CBA/J)F2 oocytes, as described elsewhere.⁽²¹⁾ To identify transgenic founder mice by Southern blot, DNA was isolated from tail biopsies, digested with BamHI, and hybridized with the microinjected fragment. Founder transgenic mice were bred with C57BL/6J mice to establish the various transgenic lines. TgRANKL progeny were genotyped by PCR (5'TCTTCAACTAATGGTGTACG; 5'TCTACAAGGTCAAGAGCATG).

Transgenic copy number

Copy number of the transgene was determined by quantitative real-time PCR (qPCR) using tail DNA from the TghuRANKL mice and wild-type (WT) littermates ($n = 8-9$). qPCR was performed using SsoFast EVA Green Supermix (Bio-Rad, Hercules, CA, USA) on a Rotor-Gene 6000 RT-PCR machine (Corbett Life Science, Sydney, Australia). A common pair of primers complementary to both human and mouse RANKL gene sequences was used to amplify both genes (5'ACCTGTACGCCAACATTTGC; 5'CTTGGGATTTGATGCTGGT). For each sample, the Ct value of RANKL was normalized against the mouse HuR gene (5'AGGACACAGCTTGGGCTACG; 5'CGTTCAGTGTGCTGATTGCT) and the values of both RANKL and HuR genes were extrapolated from their respective standard curves.

Quantitative expression analysis

Total RNA was extracted from various tissues using a monophasic solution of guanidine isothiocyanate and phenol according to the manufacturer's instructions (TRI Reagent, MRC, Cincinnati, OH, USA). After removal of DNA remnants with DNase I treatment (Sigma-Aldrich, St. Louis, MO, USA), first-strand cDNA was synthesized using 2 μ g of total RNA and M-MLV (Sigma-Aldrich), whereas qPCR was performed at 55°C for 35 cycles. Specific primer pairs were used for the quantitative expression analysis of human RANKL (5'ACGCGTATTTACAGCCAGTG; 5'CCCCTAAT-TGCTCCAATCTG), mouse RANKL (5'TGTACTTTCGAGCGCAGATG; 5'AGGCTTGTTCATCCTCCTG), and mouse OPG (5'CTTGCCTT-ATGGAGAGCCT; 5'TCGCTCGATTGCGAGTCT). The same primer pair used for RANKL copy number detection was also used for detecting both mouse and human RANKL expression. The samples were normalized to β 2-microglobulin expression (5'TTCTGGTGCTTGTCTCACTGA; 5'CAGTATGTTCCGGCTTCCCATTG). Relative expression was calculated as the fold difference compared with control values using Bio-Rad RelQuant. For each experiment, two technical and three biological replicas were used.

Histopathological analysis

Femurs and tibias were fixed in 4% paraformaldehyde (PFA) for 6 hours, decalcified in 13% EDTA, and embedded in paraffin.

Sections of 5- μ m thickness were stained with hematoxylin/eosin. Osteoclasts were stained for TRAP activity using a leukocyte acid phosphatase (TRAP) kit (Sigma-Aldrich). Nondecalcified bones were embedded in methyl methacrylate, and stained for Von Kossa to visualize mineralized bone. For assessment of bone formation, mice were injected with 100 μ L calcein (5 mg/mL), 6 and 2 days before euthanization, and undecalcified bones were embedded in methyl methacrylate according to standard double-labeling protocols.⁽²²⁾ Ectopic calcification in soft tissues was detected after staining with 2% Alizarin Red S (Applichem, Gatersleben, Germany).

Serum bone markers

Serum levels of mouse tartrate-resistant acid phosphatase form 5b (TRACP-5b), an osteoclast activity marker, was measured by enzyme-linked immunosorbent assay (ELISA) according to manufacturer's instructions (Immunodiagnostic Systems, Boldon, UK). The levels of soluble human RANKL were quantified using a human RANKL Single-Plex assay kit (Millipore/Linco, St. Charles, MO, USA) with detection limit of the assay at 4.88 pg/mL.

Biochemical markers and blood analysis

Serum clinical chemistry tests (performed by Microanalysis SA, Athens, Greece), including glucose, urea, total cholesterol, creatinine, alanine aminotransferase (ALT), aspartate aminotransferase (ALT), alkaline phosphatase (ALP), phosphorus, calcium, and ionized calcium were measured using a multichannel auto analyzer (Architect c8000, Abbott Diagnostics, Abbott Park, IL, USA). Blood samples, obtained by heart puncture, were collected in EDTA-coated tubes and blood analysis was performed (by Microanalysis SA) using full automatic blood cell counter Model PCE 210 N (ERMA INC., Tokyo, Japan).

Micro-CT

Bones (femur and tibia) were fixed in PBS plus 4% paraformaldehyde (PFA) overnight at 4°C and then washed and stored in 70% ethanol. Three-dimensional microarchitecture of the distal femur from 4-week-old or 3-month-old WT and transgenic mice was evaluated using a high-resolution SkyScan1076 microtomographic imaging system (SkyScan, Kontich, Belgium). Images were acquired at 48 KeV, 200 mA with a 0.5-mm aluminum filter. Three-dimensional reconstructions (8.8 mm cubic resolution) were generated using NRecon software (SkyScan) as previously described.⁽²³⁾ For the trabecular bone regions, we assessed the bone volume fraction (BV/TV, %), trabecular number (Tb.N, mm⁻¹), trabecular separation (Tb.S, mm), and the connectivity density (Con. Dens., mm⁻³). Femoral cortical geometry was assessed in micro-computed tomography (micro-CT UCT40, Scanco Medical AG, Basserdorf, Switzerland) using 50 continuous CT slides (600 μ m) located at the femoral midshaft as previously described.⁽²⁴⁾ For cortical bone, we measured the bone volume fraction (BV/TV), cortical tissue volume (Ct.TV, mm³), bone volume (Ct.BV, mm³), marrow volume (BMV, mm³), and the average cortical width (Ct.Th, mm).

Biomechanical test

The femur was placed in the material-testing machine on two supports separated by the distance of 9.9 mm and load was applied to the middle of the shaft, thus creating a three-point bending test. The mechanical resistance to failure was tested using a servo-controlled electromechanical system (Instron 1114,

Instron Corp., High Wycombe, UK) with actuator displaced at 2 mm/min. Both displacement and load were recorded. Ultimate force (maximal load, measured in Newtons), stiffness (slope of the linear part of the curve, representing the elastic deformation, N/mm), and elastic and plastic energy (area under the curve, up to and beyond the yield point, respectively; N/mm) were calculated from the load-displacement curves.

Denosumab treatment

Denosumab at the dose of 10 mg/kg was administered subcutaneously in the medium-copy Tg5519 mice ($n = 14$, 7 females and 7 males) twice per week from the 4th week of age for a period of 6 weeks. Saline was administered in control experimental groups consisting of Tg5519 and WT littermates ($n = 14$, 7 females and 7 males per group). Body weight was recorded weekly for each mouse. At 10 weeks of age, all mice were euthanized and the long bones were collected for blinded histopathological analysis. In addition, blood was collected to assess serum TRACP-5b levels (murine ELISA, Immunodiagnostic Systems).

Statistical analysis

All results are expressed as mean \pm standard error (SE). Student's *t* test was performed to compare means between two groups, and one-way analysis of variance (ANOVA) was performed to compare means of multiple groups. Values of $p < 0.05$ were considered significant; * $p < 0.05$, ** $p \leq 0.01$, *** $p \leq 0.001$ when not otherwise specified.

Results

Generation, identification, and expression analysis in TghuRANKL mice

To achieve a correct spatial pattern of huRANKL expression in mice, a 200-kb genomic fragment containing the whole human *RANKL* gene isolated from a BAC clone was used for transgenesis (Supplemental Fig. S1A). No gene other than *RANKL* is encoded within the microinjected fragment. Four transgenic founders, Tg5516, Tg5519, Tg5520, and Tg5521, carrying the huRANKL gene (TghuRANKL) were generated with pronuclear injections as shown by Southern blot analysis after genomic digest with BamHI and hybridization with the microinjected fragment (Fig. 1A). The Tg5521 line was not further studied because the founder was mosaic for the transgene and produced a limited number of transgenic mice. The transgene copy number was calculated in the remaining three transgenic lines using a common primer pair amplifying both mouse and human genomic sequences in qPCR (Fig. 1B). The low copy Tg5516 line (1 extra copy), the medium copy Tg5519 line (10 extra copies), and the high copy Tg5520 line (27 extra copies) were further characterized. From these lines, Tg5516 and Tg5519 transmitted the transgene to offspring, whereas the Tg5520 male founder did not produce any progeny. Therefore, more extensive expression and phenotypic analysis was performed in transgenic lines Tg5516 and Tg5519.

Comparative analysis of the levels of huRANKL expression in various tissues including bone, brain, spleen, thymus, kidney, lung, heart, and liver revealed that the medium copy Tg5519 line expressed huRANKL at significantly higher levels relative to the low copy Tg5516 line (Fig. 1C). More specifically, Tg5519 mice overexpressed huRANKL in all tissues studied, with higher levels in bone, brain, spleen, and kidney. Notably, in both TghuRANKL

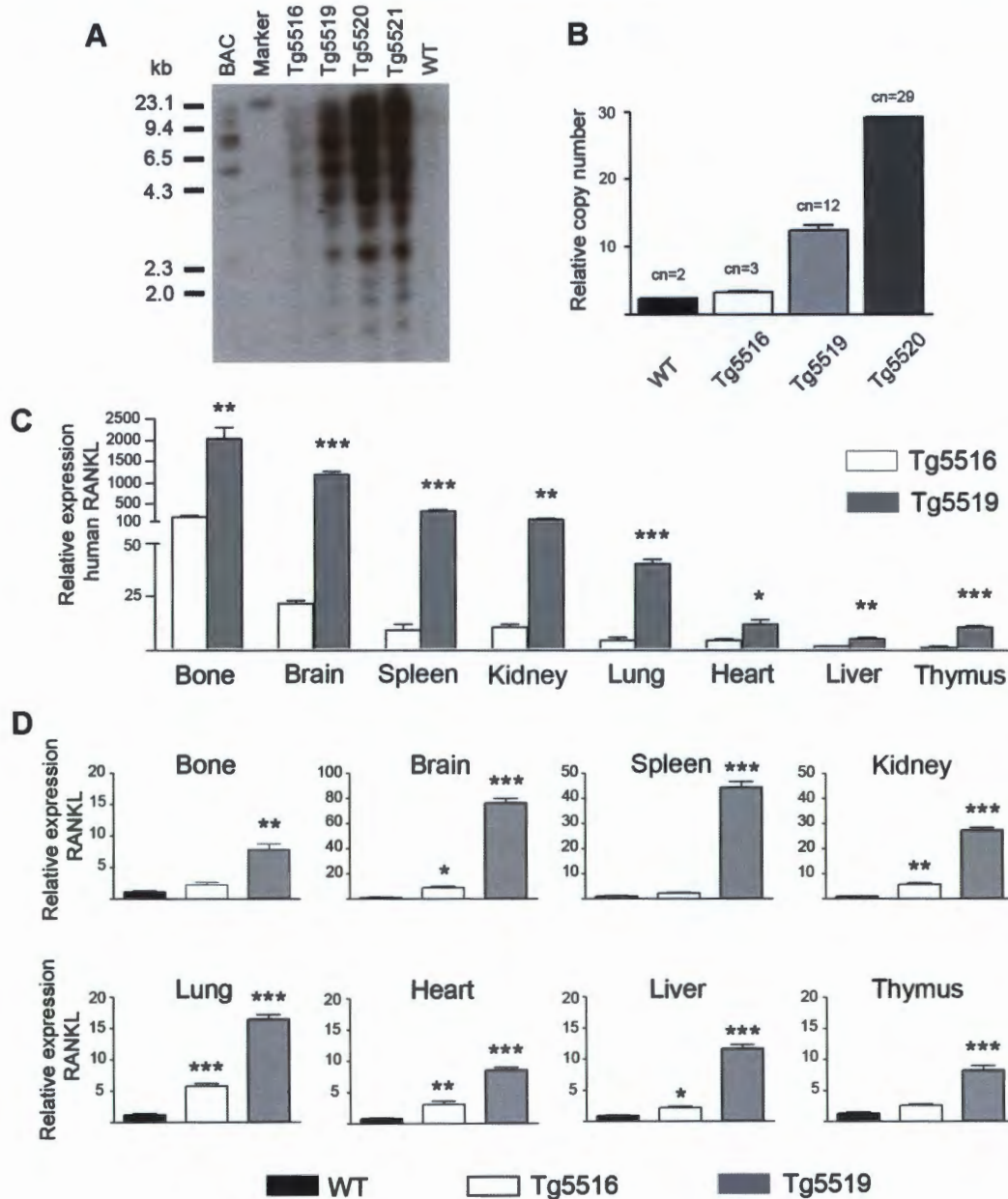


Fig. 1. Generation of huRANKL transgenic mice and comparative expression analysis. (A) Southern blot analysis on genomic DNA isolated from TghuRANKL founder and WT control mice. BAC digest was used as a positive control, whereas known molecular weights are indicated in kilobases (kb). (B) Copy number (cn) of the integrated transgenes and the endogenous mouse RANKL in WT, Tg5516, and Tg5519 mice ($n = 8-9$ per group) as well as in the Tg5520 founder. Comparative analysis of the expression levels of huRANKL (C) as well as of both human and mouse RANKL (D) in various tissues from Tg5516, Tg5519, and WT mice by qPCR ($n = 3$ per group). The expression levels of RANKL in transgenic tissues were statistically compared with endogenous RANKL levels in WT mice (D). Relative fold change of RANKL mRNA expression was normalized against $\beta 2$ -microglobulin mRNA. Mean \pm SE; * $p < 0.05$, ** $p < 0.01$, *** $p < 0.001$.

lines the levels of huRANKL were dramatically increased in bone tissue, isolated from femurs and tibias after removal of bone marrow cells, in accordance with recent studies showing that osteocytes, former osteoblasts trapped in the bone matrix, are the major source of RANKL production.⁽²⁵⁾ Importantly from a pathophysiology perspective, the pattern of huRANKL expression in various tissues from both transgenic lines closely followed the pattern of endogenous RANKL expression seen in WT mice (Supplemental Fig. S1B). To enable comparison of the levels of

the huRANKL transgene in various tissues of TghuRANKL mice with those of the endogenous mouse RANKL in WT mice, a common primer pair recognizing both mouse and human RANKL cDNA was used in qPCR. Such relative expression analysis showed that the low copy Tg5516 line expressed RANKL at significantly higher levels compared with WT mice but much lower in comparison to the medium copy Tg5519 line (Fig. 1D), confirming our previous results based on huRANKL expression (Fig. 1C).

To investigate whether the increased levels of huRANKL expression in transgenic mice influenced expression at the levels of endogenous mouse RANKL, we performed a similar analysis in tissues overexpressing huRANKL such as bone and spleen (Supplemental Fig. S1C) using a primer pair that specifically amplifies mouse RANKL cDNA. Our results showed that the levels of mouse RANKL expression in such tissues were comparable between TghuRANKL and WT control mice, indicating that the overexpression of huRANKL and the subsequent pathology had no effect in enhancing or suppressing endogenous mouse RANKL mRNA expression. Moreover, increased levels of endogenous OPG expression were detected in bone tissues from Tg5519 mice compared with Tg5516 and WT control mice, probably as a result of a negative feedback mechanism in response to huRANKL overexpression (Supplemental Fig. S1D). The high copy Tg5520 founder also overexpressed huRANKL at all tissues studied (data not shown). At the protein level, the serum levels of soluble huRANKL protein were dramatically increased in the Tg5519 line ($1065 \text{ pg/mL} \pm 151$, $n = 11$) and the Tg5520 founder (1003 pg/mL) compared with Tg5516 mice ($6.27 \text{ pg/mL} \pm 0.84$, $n = 7$) and WT control mice (undetectable, $n = 11$).

Low huRANKL-expressing Tg5516 mice develop trabecular bone loss

The low copy number Tg5516 mice were indistinguishable in appearance and average weight from WT littermates. Similarly, no hematological or biochemical abnormalities were observed in Tg5516 mice (Supplemental Tables S1 and S2). Histopathological and quantitative micro-CT analysis of the metaphyseal region of distal femurs in Tg5516 mice showed trabecular bone loss that was subtle at 4 weeks of age (Supplemental Fig. S2A, B) and pronounced at 2 (Supplemental Fig. S2A) and 3 months of age (Supplemental Fig. S2A, Fig. 2A) in both males and females. Trabecular bone volume fraction (BV/TV) was reduced nearly 2.5-fold, and trabecular number (Tb.N) was reduced more than 50% in 3-month-old Tg5516 mice compared with WT controls (Fig. 2A). Furthermore, Tg5516 mice had significantly wider trabecular separation (245%) than WT mice, whereas the connectivity density was decreased by sixfold. In contrast, the mid-diaphysis cortical bone volume (Ct.BV) and thickness (Ct.Th) were similar in Tg5516 mice and WT controls as assessed by micro-CT analysis (Fig. 2B, C). Notably, mid-diaphysis femurs from 3-month-old Tg5516 mice had reduced biomechanical

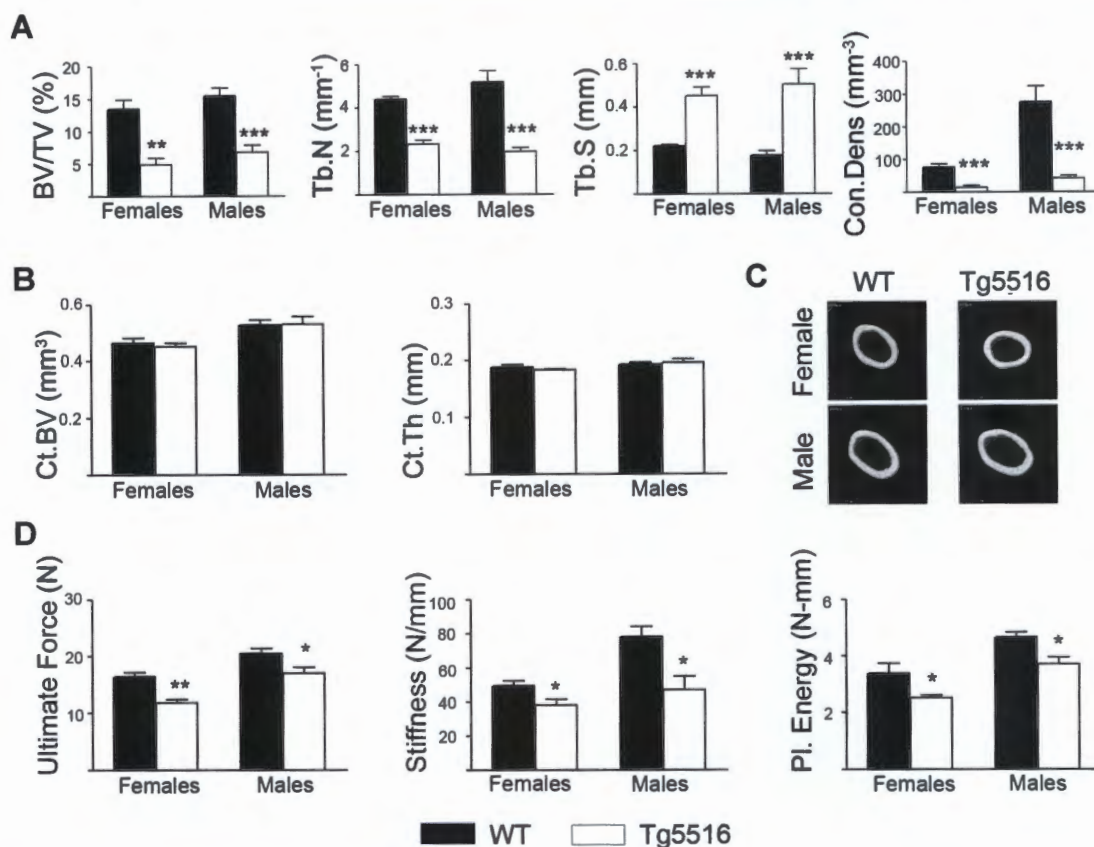


Fig. 2. Low-expressing Tg5516 mice developed trabecular bone loss and increased bone fragility. (A) Quantitative analysis of the trabecular bone in the metaphyseal region of the distal femurs in 3-month-old ($n = 5-6$ per sex) Tg5516 and WT female and male littermates with micro-CT. BV/TV (bone volume/total volume, %), Tb.N (trabecular number per mm), Tb.S (trabecular separation, mm), Con.Dens. (connectivity density, mm^{-3}). (B) Quantitative analysis of midshaft cortical bone in femurs from 3-month-old Tg5516 and WT control females and males with micro-CT ($n = 5$ per sex). Ct.BV (cortical bone volume, mm^3), Ct.Th (cortical thickness, mm). (C) Representative micro-CT 3D cortical reconstructions of mid-diaphysis cortical bone in femurs from Tg5516 and WT mice. (D) Changes in the biomechanical parameters of the femurs from 3-month-old Tg5516 and WT control mice ($n = 5$ per sex). Ultimate force (N); stiffness (N/mm); plastic energy (N-mm). Mean \pm SE; * $p < 0.05$, ** $p \leq 0.01$, *** $p \leq 0.001$.

properties such as ultimate force (−22%), stiffness (−34%), and plastic energy (−23%) as assessed by three-point bending tests (Fig. 2D). Biochemical markers of bone turnover such as TRACP-5b were normal as well as serum alkaline phosphatase levels (Supplemental Table S2). These results demonstrate that the low huRANKL-expressing Tg5516 mice develop a mild osteoporotic phenotype characterized by trabecular bone loss and decreased bone strength in both males and females by the third month of age.

Tg5519 mice overexpressing huRANKL develop severe osteoporosis

Overexpression of huRANKL in Tg5519 mice led to severe bone loss that was already established from the first month of age in both males and females. Histologically, the metaphyseal regions of the distal femur and the proximal tibia were profoundly osteoporotic in the Tg5519 mice, exhibiting an almost complete absence of trabeculae by 3 months of age (Fig. 3A), which precluded quantitative bone measurements through micro-CT analysis. Cartilage abnormalities were also observed through the accumulation of cartilaginous remnants (shown as asterisks) mainly in the epiphysis of 4-week-old (Fig. 3A) and the metaphysis of 3-month-old Tg5519 mice (Fig. 3B), which gradually disappeared. No obvious disorganization of the growth plate of 1- or 2-month-old Tg5519 mice was observed and the thickness of the various zones appeared similar to WT littermates. However, cellular density in the resting/proliferation zones appeared increased along with proliferation of the cartilaginous remnants in the epiphysis subjacent to the growth plate. Interestingly, Tg5519 mice displayed a progressive growth plate loss, already evident at 3 months of age, which almost disappeared by the age of 10 months (Fig. 3A). Growth retardation was not noticed in Tg5519 mice, even though the femoral length was modestly decreased in 3-month-old Tg5519 mice compared with WT controls (Supplemental Fig. S3). Staining of femurs with tartrate-resistant acid phosphatase (TRAP), an enzyme that is highly expressed in osteoclasts, revealed increased number of giant osteoclasts in 3-month-old Tg5519 mice both at epiphysis (Fig. 3B) as well as the mid-diaphysis cortical region (Fig. 3C).

The skeletal phenotype of the Tg5519 line was also pronounced in cortical bone. Histopathological analysis of cortical bone at the mid-diaphysis showed that Tg5519 mice had severe intracortical porosity when compared with WT littermates at 3 months of age (Fig. 3C). Von Kossa staining of undecalcified femur sections confirmed the presence of intracortical pores (Fig. 3D). Moreover, abundant fluorochrome incorporation, an index of intracortical (endosteal) bone formation, was identified in cortical bone of Tg5519 femoral diaphysis using the calcein double-labeling technique (Fig. 3E), suggesting the presence of woven bone. In addition, abundant osteoclasts were present within the cortical bone area of Tg5519 mice as opposed to WT cortical bones (Fig. 3C), indicating increased cortical bone remodeling. To confirm the presence of increased bone turnover in Tg5519 mice, we further evaluated the levels of serum biomarkers. The levels of serum alkaline phosphatase (ALP), a marker of bone formation activity, was 2.5-fold increased in 4-week-old Tg5519 mice and nearly 10-fold in 3-month-old Tg5519 mice in comparison to WT control mice (Supplemental Fig. S4A), reflecting disease severity. As expected, the serum levels of TRACP-5b were also dramatically increased in 3-month-old Tg5519 mice compared with WT control mice

(31.34 ± 1.2 versus 8.74 ± 0.6), indicating active bone resorption (Supplemental Fig. S4B).

Cortical bone loss and cortical porosity increased progressively throughout life (Supplemental Fig. S5A). Micro-CT analysis of cortical bone at the mid-diaphysis confirmed the presence of intracortical porosity in 3-month-old Tg5519 mice (Fig. 4A). Tg5519 mice ($n = 11$) exhibited a significant decrease in cortical bone volume (Ct.BV, −26%), cortical bone volume fraction (BV/TV, −38%), and cortical thickness (−48%) compared with WT control mice (Fig. 4B). Interestingly, femurs of Tg5519 mice (Fig. 4A, B) display a significant increase in the bone marrow volume (BMV, +67%) and the cortical total volume (Ct.TV, +26%) relative to WT littermates, indicating an increase in the bone width compared with WT mice. As expected, mid-diaphysis femurs from 3-month-old Tg5519 mice ($n = 10$) displayed significant reduced biomechanical properties such as ultimate force (−58%), stiffness (−70%), and plastic energy (−45%) relative to WT littermates as assessed by three-point bending tests (Fig. 4C).

To investigate the disease status at an earlier time point, we assessed both the metaphyseal trabecular region of distal femurs and the cortical bone parameters in 4-week-old Tg5519 mice through micro-CT. Our results showed that by the 4th week of age there was already substantial trabecular bone loss (Supplemental Fig. S5B). Moreover, the extent of cortical porosity was quantified in two different cortical regions, near growth plate (Supplemental Fig. S5C) and at mid-diaphysis (Supplemental Fig. S5D), showing more increased cortical porosity near growth plate. Because mid-diaphysis is already severely affected at the age of 3 months (Fig. 4B), it appears that during disease progression the cortical porosity was extended from metaphysis toward diaphysis. Moreover, the cortical bone was mainly characterized by open porosity (Supplemental Fig. S5C, D) implying a direct interaction with the bone marrow cells that probably contributed to the recruitment and maturation of osteoclast precursors. Collectively, these results indicate that huRANKL overexpression resulted in increased bone remodeling and “trabecularization” of the cortical bone.

Apart from the severe bone phenotype, histological analysis also revealed progressively increased adipocyte numbers in bone marrow of Tg5519 mice apparent from the third month of age (Fig. 3A, Supplemental Fig. S5A). Increased marrow adiposity was inversely correlated with bone marrow cellularity in Tg5519 mice from the 6th month of age (data not shown). Despite the severe bone phenotype, the Tg5519 mice appeared normal and no clinical chemistry abnormalities (Supplemental Table S2) other than elevated alkaline phosphatase levels were observed. Similarly to Tg5516 mice, no hematological abnormalities (Supplemental Table S1) were observed in Tg5519 mice. In addition, no gross histopathological lesions were detected in Tg5519 mice with the exception of few scattered peribronchial inflammatory foci observed in the lungs of 3-month-old Tg5519 mice (Supplemental Fig. S6). Soft tissue calcification was not observed in Tg5519 mice (data not shown).

Severe osteoporosis and soft tissue calcification in the high copy Tg5520 founder

The high copy Tg5520 founder (Fig. 1B) overexpressing huRANKL exhibited progressive kyphosis indicating severe osteoporosis and never gave progenies probably because of the severe skeletal phenotype. At 8 months of age, the Tg5520 founder was euthanized and the tissues were assessed histologically. Histological examination of the metaphyseal distal femurs

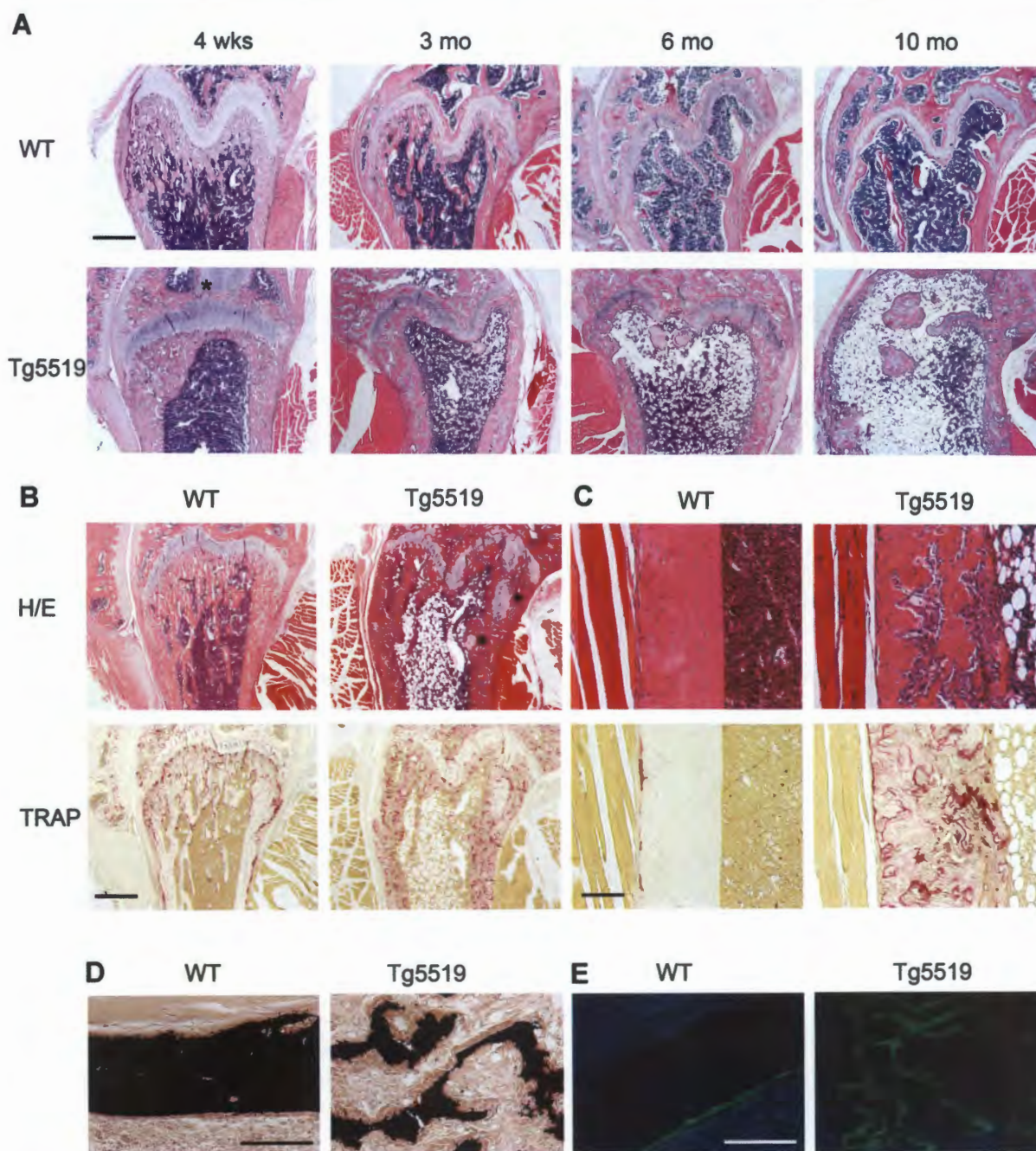


Fig. 3. Tg5519 mice overexpressing huRANKL developed trabecular bone loss, growth plate loss, marrow adiposity, increased osteoclastogenesis, intracortical porosity, and increased cortical bone remodeling. (A) Representative sections of metaphyseal distal femurs from 4-week-, 3-month-, 6-month-, and 10-month-old Tg5519 mice and WT littermates, stained with hematoxylin/eosin (H/E) ($n = 6$). Scale bar = 500 μm . (B) Representative serial sections of distal femurs from 3-month-old Tg5519 and WT controls stained with H/E and TRAP ($n = 6$). Scale bar = 500 μm . (C) Cortical bone porosity with increased osteoclastogenesis in 3-month-old Tg5519 mice. Representative serial sections of mid-diaphysis cortical bone stained with H/E and TRAP ($n = 6$). Scale bar = 100 μm . (D) Von Kossa staining of cortical bone and (E) double calcein labeling in 3-month-old Tg5519 and WT mice. Asterisks indicate cartilage remnants in Tg5519 mice (A, B). Scale bar = 100 μm .

revealed absence of trabecular bone, growth plate loss, and bone fractures (Fig. 5A). Tg5520 founder also developed intracortical porosity, giant osteoclasts inside the cortical area (Fig. 5B), and increased marrow adiposity (Fig. 5A, B) similarly to Tg5519 mice. Interestingly, ectopic calcification was observed in soft tissues

like kidney (Fig. 5C), heart (Fig. 5D), lung (Fig. 5E), and tongue (Fig. 5F) of the Tg5520 founder compared with WT control (Supplemental Fig. S7), as revealed by staining with hematoxylin/eosin and Alizarin red, which specifically stains calcium phosphate deposits.

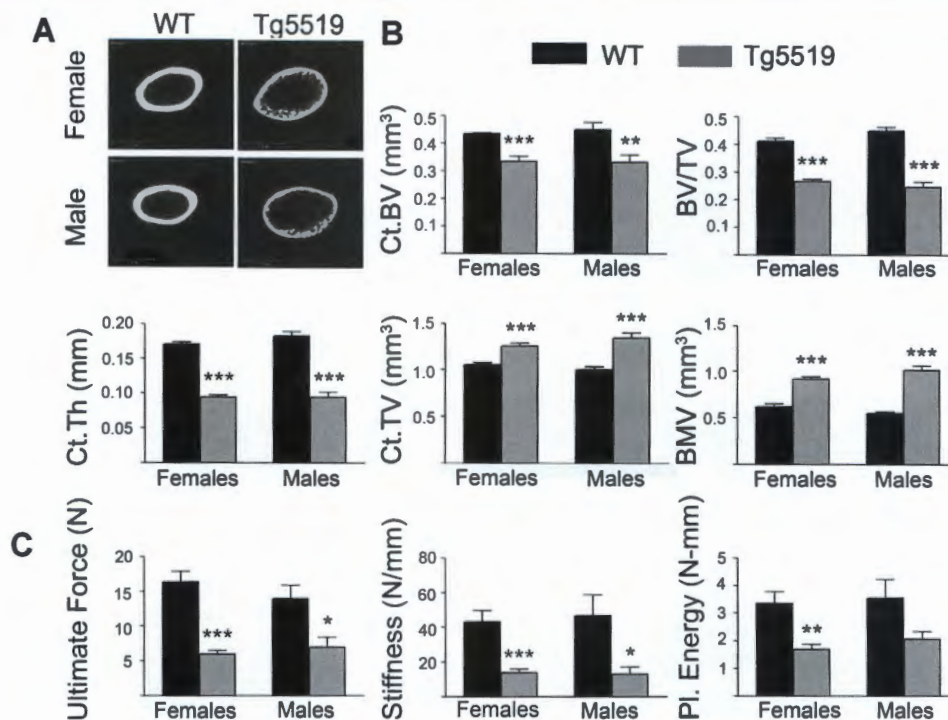


Fig. 4. Tg5519 mice developed cortical porosity and increased bone fragility. (A) Representative micro-CT 3D cortical reconstructions and (B) quantitative analysis of mid-diaphysis cortical bone in femurs from 3-month-old Tg5519 and WT mice with micro-CT ($n = 6$ for females and $n = 5$ for males). Ct.BV (cortical bone volume, mm^3), BV/TV (bone volume/total volume), Ct.Th (cortical thickness, mm), Ct.TV (cortical total volume/ mm^3), BMV (bone marrow volume/ mm^3). (C) Altered biomechanical parameters of the femurs from 3-month-old Tg5519 and WT mice. Ultimate force (N); stiffness (N/mm); plastic energy (N-mm) ($n = 6$ for females and $n = 4$ for males). Mean \pm SE; * $p < 0.05$, ** $p \leq 0.01$, *** $p \leq 0.001$.

Transgenic rescue of RANKL-mediated osteopetrosis

Subsequently, we investigated whether the huRANKL transgene was sufficient to rescue RANKL-mediated osteopetrosis. In the past, we identified a recessive loss-of-function *Rankl* allele in *Rankl*^{ties/ties} mice, causing severe osteopetrosis, failure of tooth eruption, defective lymph node organogenesis, and premature lethality similarly to *Rankl*-deficient mice.⁽²⁰⁾ Introduction of a low copy huRANKL transgene into the *Rankl*^{ties/ties} genome through crossings with the Tg5516 line fully restored survival (not shown), body weight gain, and eruption of the lower incisors, although eruption of upper incisors was partial (Supplemental Fig. S8A, B). Moreover, the osteopetrotic phenotype was rescued as shown by the presence of fully expanded bone marrow cavities in the long bones of Tg5516/*Rankl*^{ties/ties} mice (Supplemental Fig. S8C). However, the partial rescue of the tooth eruption (Supplemental Fig. S8B) as well as failure of lymph node organogenesis (Supplemental Fig. S8D) noticed in Tg5516/*Rankl*^{ties/ties} mice indicate that the low copy huRANKL transgene did not completely rescue the phenotype caused by a loss-of-function mouse *Rankl* allele. In contrast, a medium copy huRANKL transgene in Tg5519/*Rankl*^{ties/ties} mice rescued the clinical signs (Supplemental Fig. S8A) and the osteopetrotic phenotype (Supplemental Fig. S8C) of the *Rankl*^{ties/ties} mice, including restoration of tooth eruption (Supplemental Fig. S8B) and mesenteric lymph nodes organogenesis (Supplemental Fig. S8D). Collectively, these results indicate that the levels and pattern of huRANKL expression in transgenic lines are adequate for the restoration of the osteopetrotic phenotype. Moreover, our

data show that the huRANKL transgene is fully active in mice, implying full activation of the mouse RANK receptor.

Denosumab treatment inhibits bone resorption in Tg5519 mice

We further investigated whether the severe osteoporotic phenotype developed in Tg5519 mice could be suppressed and restored by denosumab, a human monoclonal antibody against human RANKL. Denosumab, at 10 mg/kg, was administered subcutaneously in Tg5519 mice ($n = 14$) for a period of 6 weeks starting from the 4th week of age where bone resorption was already established both at the trabecular and the cortical areas. Saline-treated WT and Tg5519 littermates were included to assess physiological bone structure and disease progression during the treatment period, respectively. Histological analysis of distal femurs from saline-treated Tg5519 mice showed remarkable trabecular bone loss at 10 weeks of age, whereas treatment with denosumab resulted in preservation of trabecular bone in the metaphyses of Tg5519 mice (Fig. 6A). Moreover, the cortical porosity and the increased intracortical osteoclastogenesis developed in Tg5519 littermates were completely suppressed upon denosumab treatment (Fig. 6B). Denosumab treatment also fully reversed the increased serum levels of TRACP-5b in Tg5519 mice back to the levels of WT littermates (Fig. 6C). Overall, these results demonstrate that the specific inhibition of human RANKL by denosumab treatment substantially reversed the severe osteoporotic phenotype of Tg5519 mice.

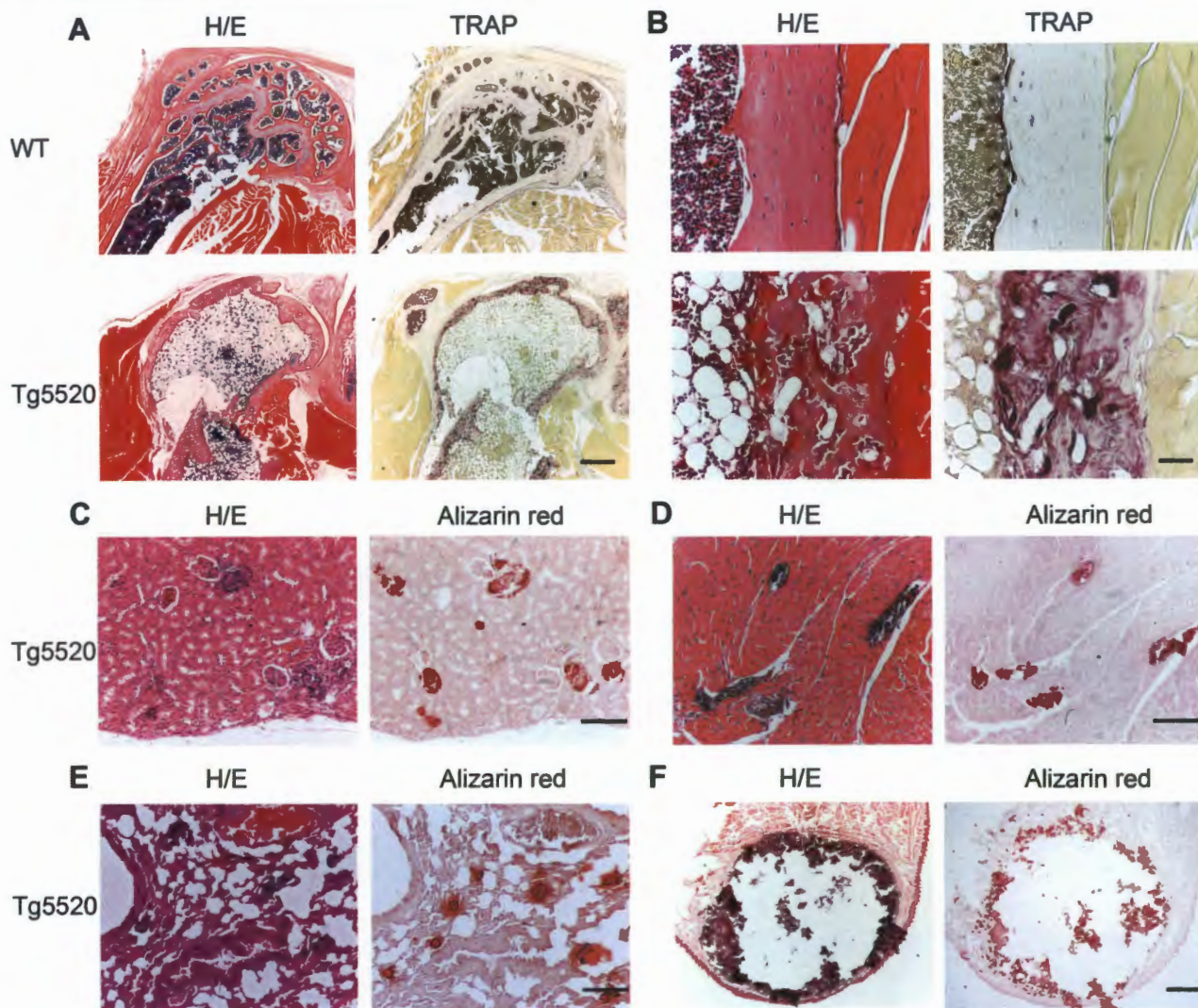


Fig. 5. High copy number Tg5520 founder developed trabecular and growth plate loss, cortical porosity, and soft tissue calcification. (A) Serial sections of metaphyseal distal femurs and (B) mid-diaphysis cortical bone from 8-month-old Tg5520 founder and WT control, stained with hematoxylin/eosin (H/E) and TRAP showed loss of trabecular bone and growth plate, fractures, cortical porosity, and giant osteoclasts. (C) Serial sections of kidney, (D) heart, (E) lung, and (F) tongue from the Tg5520 founder stained with hematoxylin/eosin (H/E) and alizarin red showed ectopic calcification. Scale bars: A, F = 500 μ m; B = 50 μ m; C, D = 100 μ m.

Discussion

In the current study, we report the generation and characterization of novel osteoporosis models by overexpression of huRANKL in transgenic mice carrying the human RANKL genomic locus. The gene structure of RANKL is highly conserved in mammals, consisting of 5 exons that span 33.9 kb in humans and 30.5 kb in mice, whereas RANKL homologues have been identified so far only in organisms that contain osteoclasts, ie, vertebrates. In mammals, the transcription of RANKL is controlled by multiple transcriptional enhancers, some of which reside in long distance, more than 70 kb, upstream from the transcription start site.⁽⁹⁾ To achieve a physiologically relevant expression pattern of RANKL overexpression, a 200-kb genomic region, isolated from a BAC library, spanning the coding region as well as the regulatory sites of the huRANKL gene was used for microinjections into the

pronucleus of fertilized eggs. Large genomic transgenes derived from BAC clones are more likely to provide physiologically relevant expression patterns and copy dependent expression levels, regardless of position effects.⁽²⁶⁾ These effects were also verified in the TghuRANKL lines as the levels of huRANKL expression in various tissues were analogous to the transgene copy number and followed the expression pattern of endogenous mouse RANKL gene. Mice from the low copy Tg5516 line expressed huRANKL in higher levels compared with WT littermates but much lower levels relative to the medium copy Tg5519 line. Previous studies have shown that RANKL is widely expressed in a variety of cell types both in skeletal and extraskeletal tissues.⁽⁸⁾ Our studies showed that mice from both TghuRANKL lines, Tg5516 and Tg5519, overexpressed huRANKL in all tissues shown to express endogenous RANKL in the WT controls. Notably, huRANKL was more highly expressed

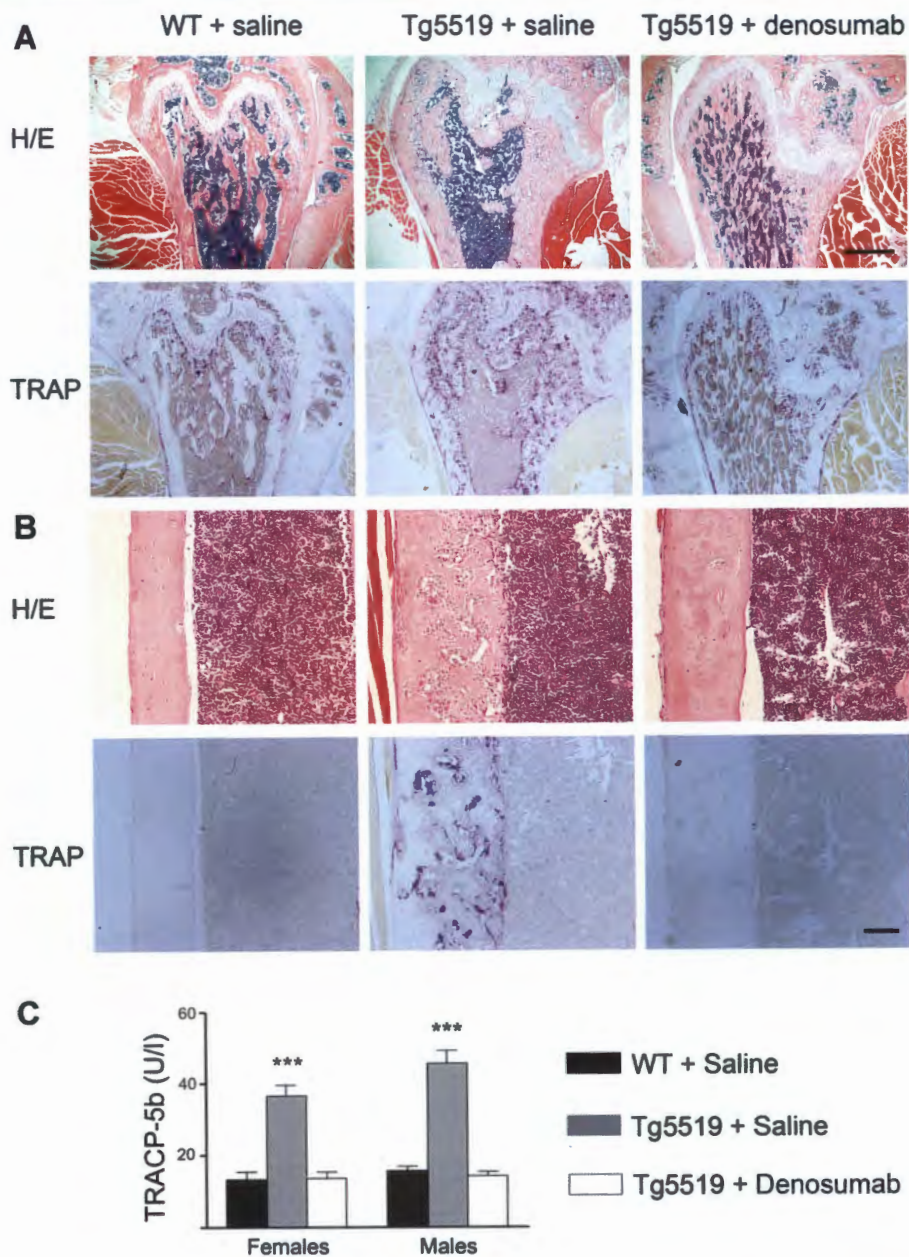


Fig. 6. Therapeutic effects of denosumab in Tg5519 mice. Representative serial sections of metaphyseal distal femur (A) and mid-diaphysis cortical bone (B) stained with hematoxylin/eosin (H/E) and TRAP from Tg5519 mice treated either with saline or denosumab and WT littermates treated with saline ($n = 14$ mice per group). Scale bars: A = 500 μm ; B = 100 μm . (C) Serum TRACP-5b levels in Tg5519 mice treated with denosumab compared with those in saline-treated WT and Tg5519 littermates ($n = 14$ per group). Mean \pm SE; *** $p \leq 0.001$.

in the bone tissue, in accordance with recent genetic studies in mice revealing that osteocytes are the major source of RANKL production,⁽²⁵⁾ stimulating osteoclast formation and remodeling. Further studies assessing the effect of huRANKL overexpression in extraskeletal tissues such as the brain and the immune system in Tg5519 mice could reveal novel pathological implications.

TghuRANKL mice overexpressing human RANKL exhibited an early-onset osteoporotic phenotype in both sexes. Tg5516 mice expressing human RANKL at low levels displayed significant trabecular bone loss already established at the second month of age and reduced biomechanical properties compared with WT controls. In contrast, the cortical bone parameters as well as the serum bone remodeling markers measured were similar

between Tg5516 mice and WT mice, indicating the development of a mild osteoporotic phenotype. On the other hand, greater overexpression of human RANKL in the Tg5519 line resulted in severe osteoporosis characterized by lack of trabecular bones, destruction of the growth plate, and severe cortical bone porosity in the femur accompanied by decreased bone strength compared with WT littermates. Chondrocytes are presumably overexpressing RANKL, and either this source, or other sources, is promoting chondroclasis and growth plate loss that ultimately diminishes longitudinal bone growth. Osteoclast formation at the intracortical surfaces as well as serum markers of bone turnover such as TRACP-5b were progressively increased in Tg5519 mice, indicating active bone resorption. Tg5519 mice

also displayed active bone formation and significantly increased serum alkaline phosphatase levels, which is consistent with increased remodeling activation that leads to osteoblast-mediated refilling of a great number or volume of resorption spaces. Cortical porosity, the result of intracortical bone resorption, was particularly pronounced in the Tg5519 line. In humans, cortical porosity increases during aging and osteoporosis progression⁽²⁷⁾ and is associated with decreased bone strength and may contribute to the increased fracture risk in such patients. Thus, the Tg5519 mice represent a unique animal model for the investigation of the pathogenetic mechanisms in cortical porosity as well as the evaluation of novel therapies through parallel analyses of both trabecular and cortical bone sites.

In addition, Tg5519 mice developed a progressive increase in bone marrow adipocytes. In humans, accelerated marrow adiposity has been associated with aging and osteoporosis.⁽²⁸⁾ Previous studies have shown an inverse association between bone marrow adiposity and bone mineral density,⁽²⁹⁾ since osteoblasts and adipocytes are thought to differentiate from the same mesenchymal stem cells. Adipocyte infiltration into the bone marrow occurs during aging and estrogen deficiency as a result of increased adipogenesis within the bone marrow at the expense of osteoblastogenesis.^(30,31) However, the causal role of increased bone marrow fat in regulating bone density remains ambiguous. The progressive marrow adiposity observed in 3-month-old Tg5519 mice accompanied the increased bone remodeling established already from the 4th week of age. Thus, our study indicates that the increase in marrow adiposity does not precede bone resorption but rather emerges after disease occurrence. The hematopoietic-to-adipogenic transition is certainly another interesting phenotype of the Tg5519 mice, which could be used to gain mechanistic insights into the role of RANKL in this phenomenon.

Tg5519 mice displayed phenotypic similarities with the OPG-deficient mice including early onset of trabecular bone loss, progressive growth plate destruction, cortical porosity, and increased bone remodeling.⁽¹²⁾ In both cases, elevated serum alkaline phosphatase levels and greater quantity of fluorescent label in the cortical bone probably reflect the coupling of bone formation to bone resorption within the basic multicellular remodeling unit. However, compared with the high-expressing Tg5519 mice, OPG-deficient mice exhibited an even more severe skeletal phenotype. OPG-deficient mice also displayed medial calcification of the aorta and renal arteries⁽¹²⁾ that was not apparent in Tg5519 mice. The effect of RANKL in vascular calcification remains somewhat ambiguous because of the opposing results derived from different studies,^(32,33) but RANKL inhibitors including denosumab have been shown to inhibit vascular calcification in several animal models.⁽³⁴⁾ The high copy Tg5520 founder did exhibit extensive calcification in soft tissues like kidney, lung, heart, and tongue, which might be the first evidence that systemic RANKL overexpression can cause soft tissue calcification.

Previous studies attempting to restore RANKL-mediated osteopetrosis through administration of soluble mouse RANKL⁽³⁵⁾ or transgenic expression of mouse RANKL in T and B lymphocytes resulted in partial rescuing.⁽³⁶⁾ Similarly, our results showed partial restoration of the RANKL-mediated osteopetrotic phenotype in the presence of a low copy huRANKL transgene but complete rescue of the skeletal and lymph node organogenesis phenotype upon huRANKL overexpression in Tg5519/*Rankl*^{fl^{es}/fl^{es}} mice. These results indicate that the levels and pattern of

huRANKL expression in transgenic lines are adequate for the restoration of the osteopetrotic phenotype, and could be further exploited for the development of novel therapeutic approaches that target cell-based local delivery of RANKL in ARO.

Previous preclinical studies assessing the efficacy and safety of denosumab in animal models have been restricted so far to cynomolgus monkeys^(17,37) as well as to knock-in mice expressing a chimeric murine/human RANKL.⁽¹⁸⁾ A significant limitation of those chimeric knock-in mice is that their remodeling rate is lower and their bone mass higher than WT controls, which limits their utility for osteoporosis research. In contrast, the TghuRANKL mice exhibit early-onset osteoporosis secondary to greatly increased remodeling rate. Our results confirmed that inhibition of huRANKL by denosumab in Tg5519-treated mice not only prevented bone loss progression but also fully restored the "osteoporotic" trabecular and cortical bone structure. Further validating the TghuRANKL model, denosumab decreased serum TRACP-5b to the level of WT controls, indicating normal activity of their endogenous RANKL.

Collectively, our TghuRANKL mice constitute the first transgenic models of early-onset osteoporosis attributable to human RANKL overexpression and thus offer a unique system for understanding the pathogenesis of high-turnover bone diseases and for the preclinical evaluation of novel huRANKL inhibitors. In addition, further studies on TghuRANKL mice might reveal novel extraskeletal pathologies associated with RANKL overexpression.

Disclosures

PK, MS, and C-YH are employed by and may own stock or stock options in Amgen, Inc. All other authors state that they have no conflicts of interest.

Acknowledgments

We thank Nikos Karoulias (Amgen Hellas Pharmaceutical E.P.E) for critical discussions and support. We also thank the AniRA facility from SFR Biosciences (UMS3444/US8) for their support and expertise and Dr Rogely Boyce (Amgen, Inc.) for histopathological evaluation of the growth plate structure. This work was funded by the project TheRAlead (09ΣYN-21-784, to ED), which is cofinanced by the European Union (European Regional Development Fund [ERDF]) and Greek national funds through the Operational Program "Competitiveness & Entrepreneurship," NSRF 2007–2013 in the context of GSRT-National action "Cooperation." This work was also supported by the Public Benefit Foundation John S. Latsis (grant number 2010–16 to ED), the Initial Training Network (ITN) Osteoimmune (grant 289150 to ED) funded by the EC 7th Framework Program and SNF grant 310030-146294 (to SF). This research has been cofinanced by the European Union (European Social Fund [ESF]) and Greek national funds through the Operational Program "Education and Lifelong Learning" of the National Strategic Reference Framework (NSRF) Research Funding Program: Heracleitus II. Investing in knowledge society through the European Social Fund.

Authors' roles: VR, AN, and ED performed the research. RD and NB performed the micro-CT analysis. NB also performed the biomechanical tests. MS and CYH performed the TRACP-5b in Tg5519-treated mice. PK, PJ, and SF reviewed the intermediate draft. ED designed the study, performed the literature review, prepared the initial and final versions of the paper, and submitted the document.

References

1. Karsenty G, Wagner EF. Reaching a genetic and molecular understanding of skeletal development. *Dev Cell*. 2002;2(4):389–406.
2. Darby AJ. Bone formation and resorption in postmenopausal osteoporosis. *Lancet*. 1981;2(8245):536.
3. Fuller K, Wong B, Fox S, Choi Y, Chambers TJ. TRANCE is necessary and sufficient for osteoblast-mediated activation of bone resorption in osteoclasts. *J Exp Med*. 1998;188(5):997–1001.
4. Leibbrandt A, Penninger JM. RANK/RANKL: regulators of immune responses and bone physiology. *Ann NY Acad Sci*. 2008;1143:123–50.
5. Lacey DL, Timms E, Tan HL, et al. Osteoprotegerin ligand is a cytokine that regulates osteoclast differentiation and activation. *Cell*. 1998;93(2):165–76.
6. Lacey DL, Tan HL, Lu J, et al. Osteoprotegerin ligand modulates murine osteoclast survival in vitro and in vivo. *Am J Pathol*. 2000;157(2):435–48.
7. Luan X, Lu Q, Jiang Y, et al. Crystal structure of human RANKL complexed with its decoy receptor osteoprotegerin. *J Immunol*. 2012;189(1):245–52.
8. Kartsogiannis V, Zhou H, Horwood NJ, et al. Localization of RANKL (receptor activator of NF kappa B ligand) mRNA and protein in skeletal and extraskeletal tissues. *Bone*. 1999;25(5):525–34.
9. O'Brien CA. Control of RANKL gene expression. *Bone*. 2010;46(4):911–9.
10. Hanada R, Hanada T, Sigl V, Schramek D, Penninger JM. RANKL/RANK-beyond bones. *J Mol Med (Berl)*. 2011;89(7):647–56.
11. Lo Iacono N, Pangrazio A, Abinun M, et al. RANKL cytokine: from pioneer of the osteoimmunology era to cure for a rare disease. *Clin Dev Immunol*. 2013;2013:412768.
12. Bucay N, Sarosi I, Dunstan CR, et al. Osteoprotegerin-deficient mice develop early onset osteoporosis and arterial calcification. *Genes Dev*. 1998;12(9):1260–8.
13. Eghbali-Fatourehchi G, Khosla S, Sanyal A, et al. Role of RANK ligand in mediating increased bone resorption in early postmenopausal women. *J Clin Invest*. 2003;111(8):1221–30.
14. Li X, Ominsky MS, Stolina M, et al. Increased RANK ligand in bone marrow of orchietomized rats and prevention of their bone loss by the RANK ligand inhibitor osteoprotegerin. *Bone*. 2009;45(4):669–76.
15. Cummings SR, San Martin J, McClung MR, et al. Denosumab for prevention of fractures in postmenopausal women with osteoporosis. *N Engl J Med*. 2009;361(8):756–65.
16. Smith MR, Egerdie B, Hernandez Toriz N, et al. Denosumab in men receiving androgen-deprivation therapy for prostate cancer. *N Engl J Med*. 2009;361(8):745–55.
17. Kostenuik PJ, Smith SY, Jollette J, Schroeder J, Pyrah I, Ominsky MS. Decreased bone remodeling and porosity are associated with improved bone strength in ovariectomized cynomolgus monkeys treated with denosumab, a fully human RANKL antibody. *Bone*. 2011;49(2):151–61.
18. Kostenuik PJ, Nguyen HQ, McCabe J, et al. Denosumab, a fully human monoclonal antibody to RANKL, inhibits bone resorption and increases BMD in knock-in mice that express chimeric (murine/human) RANKL. *J Bone Miner Res*. 2009;24(2):182–95.
19. Mizuno A, Kanno T, Hoshi M, et al. Transgenic mice overexpressing soluble osteoclast differentiation factor (sODF) exhibit severe osteoporosis. *J Bone Miner Metab*. 2002;20(6):337–44.
20. Douni E, Rintotas V, Makrinou E, et al. A RANKL G278R mutation causing osteopetrosis identifies a functional amino acid essential for trimer assembly in RANKL and TNF. *Hum Mol Genet*. 2012;21(4):784–98.
21. Douni E, Alexiou M, Kollias G. Genetic engineering in the mouse: tuning TNF/TNFR expression. *Methods Mol Med*. 2004;98:137–70.
22. Dacquin R, Davey RA, Laplace C, et al. Amylin inhibits bone resorption while the calcitonin receptor controls bone formation in vivo. *J Cell Biol*. 2004;164(4):509–14.
23. Mugniery E, Dacquin R, Marty C, et al. An activating Fgfr3 mutation affects trabecular bone formation via a paracrine mechanism during growth. *Hum Mol Genet*. 2012;21(11):2503–13.
24. Bouxsein ML, Myers KS, Shultz KL, Donahue LR, Rosen CJ, Beamer WG. Ovariectomy-induced bone loss varies among inbred strains of mice. *J Bone Miner Res*. 2005;20(7):1085–92.
25. O'Brien CA, Nakashima T, Takayanagi H. Osteocyte control of osteoclastogenesis. *Bone*. 2013;54(2):258–63.
26. Van Keuren ML, Gavrilina GB, Filipiak WE, Zeidler MG, Saunders TL. Generating transgenic mice from bacterial artificial chromosomes: transgenesis efficiency, integration and expression outcomes. *Transgenic Res*. 2009;18(5):769–85.
27. Cooper DM, Thomas CD, Clement JG, Turinsky AL, Sensen CW, Hallgrímsson B. Age-dependent change in the 3D structure of cortical porosity at the human femoral midshaft. *Bone*. 2007;40(4):957–65.
28. Rosen CJ, Klibanski A. Bone, fat, and body composition: evolving concepts in the pathogenesis of osteoporosis. *Am J Med*. 2009;122(5):409–14.
29. Li X, Kuo D, Schafer AL, et al. Quantification of vertebral bone marrow fat content using 3 Tesla MR spectroscopy: reproducibility, vertebral variation, and applications in osteoporosis. *J Magn Reson Imaging*. 2011;33(4):974–9.
30. Rosen CJ, Bouxsein ML. Mechanisms of disease: is osteoporosis the obesity of bone? *Nat Clin Pract Rheumatol*. 2006;2(1):35–43.
31. Foo C, Frey S, Yang HH, Zellweger R, Filgueira L. Downregulation of beta-catenin and transdifferentiation of human osteoblasts to adipocytes under estrogen deficiency. *Gynecol Endocrinol*. 2007;23(9):535–40.
32. Kaden JJ, Bickelhaupt S, Grobholz R, et al. Receptor activator of nuclear factor kappaB ligand and osteoprotegerin regulate aortic valve calcification. *J Mol Cell Cardiol*. 2004;36(1):57–66.
33. Tseng W, Graham LS, Geng Y, et al. PKA-induced receptor activator of NF-kappaB ligand (RANKL) expression in vascular cells mediates osteoclastogenesis but not matrix calcification. *J Biol Chem*. 2010;285(39):29925–31.
34. Helas S, Goettsch C, Schoppet M, et al. Inhibition of receptor activator of NF-kappaB ligand by denosumab attenuates vascular calcium deposition in mice. *Am J Pathol*. 2009;175(2):473–8.
35. Lo Iacono N, Blair HC, Poliani PL, et al. Osteopetrosis rescue upon RANKL administration to Rankl(-/-) mice: a new therapy for human RANKL-dependent ARO. *J Bone Miner Res*. 2012;27(12):2501–10.
36. Kim N, Odgren PR, Kim DK, Marks SC Jr, Choi Y. Diverse roles of the tumor necrosis factor family member TRANCE in skeletal physiology revealed by TRANCE deficiency and partial rescue by a lymphocyte-expressed TRANCE transgene. *Proc Natl Acad Sci USA*. 2000;97(20):10905–10.
37. Ominsky MS, Stouch B, Schroeder J, et al. Denosumab, a fully human RANKL antibody, reduced bone turnover markers and increased trabecular and cortical bone mass, density, and strength in ovariectomized cynomolgus monkeys. *Bone*. 2011;49(2):162–73.